American Mineralogist, Volume 65, pages 900–914, 1980

Solubility mechanisms of H_2O in silicate melts at high pressures and temperatures: a Raman spectroscopic study

BJØRN O. MYSEN, DAVID VIRGO, WENDY J. HARRISON AND CHRISTOPHER M. SCARFE[1]

Geophysical Laboratory, Carnegie Institution of Washington
Washington, D.C. 20008

Abstract

Raman spectroscopy has been employed to determine the solubility mechanisms of H_2O in silicate melts. In melts that have a three-dimensional network structure (*e.g.*, melts on the join Na_2O–Al_2O_3–SiO_2), water reacts with bridging oxygens to form two OH groups per broken oxygen bond. At the same time some of the three-dimensional network is broken down to chain units, accompanied by the expulsion of Al^{3+} from tetrahedral coordination. In melts that have nonbridging oxygen (NBO), water reacts with both nonbridging oxygen and network modifiers (*e.g.*, Na^+) to form Si–OH bonds and M(OH) or $M(OH)_2$ complexes. The anhydrous portion of the network becomes more polymerized.

The formation of chain units at the expense of three-dimensional network units in melts implies that the liquidus boundaries involving pyroxenes and silica minerals or feldspar minerals shift to higher silica contents. Liquidus fields of silica minerals or feldspar minerals are depressed relative to those of pyroxene minerals. This prediction is supported by published observations of phase relations in hydrous basalt and andesite systems. Similar logic can be used to explain the formation of partial melts of andesitic bulk composition from hydrous peridotite in the upper mantle.

We propose that trace-element crystal–liquid partition coefficients involving highly polymerized melts will decrease with increasing water content because of the formation of the less polymerized chain units in the melt. Partition coefficients involving less polymerized melts (*e.g.*, picrite and komatiite) may increase because the degree of polymerization of the melt is increased as a result of dissolved water.

Introduction

Water is one of the most important volatiles in magmas. The presence of H_2O in the source region of partial melts in the upper mantle results in a more silica-rich liquid than in its absence (*e.g.*, Kushiro *et al.*, 1968; Kushiro, 1969, 1972; Yoder, 1969). For this reason, for example, water is required to produce andesitic partial melts from peridotite (Kushiro *et al.*, 1972; Mysen and Boettcher, 1975). Water in magma also affects crystallization paths. The liquidus fields of feldspars are depressed relative to those of pyroxenes, and the liquidus fields of pyroxenes relative to those of olivine (Yoder, 1969, 1973; Eggler, 1972; Kushiro, 1972). The redox equilibria of iron and hence the phase equilibria of iron-bearing minerals also depend on the water content of magma (Osborn, 1959).

Physical properties of magma such as viscosity and electrical conductivity are affected by water (Lebedev and Khitarov, 1964; Kushiro, 1978; Kushiro *et al.*, 1976). It has also been suggested that activity coefficients of trace elements and therefore crystal–liquid partition coefficients depend on the water content of the liquid (Drake and Holloway, 1977; Hart and Davis, 1978).

As a result of the important petrological influence of H_2O in silicate melts, the solubility behavior of H_2O in a variety of melts and under a variety of physical conditions has been studied extensively (Goranson, 1931; Kennedy *et al.*, 1962; Burnham, 1974, 1975; Burnham and Jahns, 1962; Burnham and Davis, 1971, 1974; Hamilton *et al.*, 1964; Eggler and Rosenhauer, 1978). Solubility models of H_2O in silicate melts based on solubility data and thermodynamic properties of hydrous melts have been proposed (Burnham, 1974, 1975).

[1] On leave from the University of Alberta, Edmonton, Canada.

0003–004X/80/0910–0900$02.00

Despite the importance of H_2O in petrogenetic processes, data on the structural role of H_2O in silicate melts are scarce. Orlova (1964) and Velde and Kushiro (1976) determined that OH groups exist in highly polymerized, water-bearing melts on the join $NaAlSiO_4$–SiO_2. Hodges (1974) suggested that molecular water may occur as well. Data on the structural role of the OH groups in silicate melts are rare (Adams and Douglas, 1959). No data appear to exist for melts formed at both high temperature and high pressure. Such data are necessary to understand the influence of H_2O on chemical and physical processes of magma formation and evolution. In the present report, Raman spectroscopy has been used to determine (1) the chemical and structural forms of dissolved water in silicate melts and (2) the interaction between water-bearing structural units and the remaining anionic structure of silicate melts.

Experimental methods

The Raman spectra were acquired on small chips (~1 mm) of quenched melts. A discussion of the application of such data to the structures of melts was provided by Mysen *et al.* (1980). The problem was also discussed by Taylor and Brown (1979) and Sharma *et al.* (1978). They concluded that the structural features of liquids that are discernible with Raman spectroscopy can be quenched at least with the quenching rates employed here (250°–500°C/sec).

An added complexity in the present experiments is the mobility of H_2O in silicate melts and the tendency of water-bearing melts not to form a glass. Instead, minerals precipitate from the melt during quenching. In melts with a three-dimensional network structure [*e.g.*, $NaAlSi_2O_6$ (Jd) and $NaAlSi_3O_8$ (Ab) compositions in the present study] it has been suggested that liquids with up to about 5 wt. percent H_2O can be quenched at high pressure (Burnham, 1975). No more than about 5 wt. percent H_2O was therefore added to these melts. Whether H_2O could be quenched in these melts was also assessed by monitoring the intensity of the Si–OH and HOH stretch bands in the Raman spectra (see below).

Less is known about melts that are less polymerized than those that have a three-dimensional network (NBO/T > 0).[2] In fact hydrous melts of metasilicate composition cannot even be quenched to a glass. Di- and trisilicate of sodium [$Na_2Si_2O_5$ (NS2) and $Na_2Si_3O_7$ (NS3)] can be quenched to clear, bubble-free glass at least with water contents up to 4–5 wt. percent. Inasmuch as the intensity of Raman bands of Si–OH stretch vibrations of such melts increases with increasing H_2O content of the quenched melt, we conclude that in these melts (NS2 and NS3) the H_2O content can be quenched. Melts of $Na_2Si_2O_5$ and $Na_2Si_3O_7$ composition were used, therefore, to study solubility mechanisms of H_2O in silicate melts with a significant number of nonbridging oxygens.

The starting materials for high-pressure experiments were glasses made at 1 atm. The glasses were produced from spectroscopically pure (Johnson and Matthey) SiO_2 and Al_2O_3 and reagent-grade Na_2CO_3 (Fisher). Water was double-distilled H_2O, added to the samples with a microsyringe with 0.03 μl precision. Deuterium oxide (MSD isotope products, Canada) was 95 percent D_2O and 5 percent H_2O.

The samples were contained in sealed Pt capsules of 2 or 3 mm O.D. In order to ensure that the desired amount of water was in the charge during an experiment, the capsules were weighed before and after welding and again after 1–2 hr at 110°C. The accuracy of the amount of water reported is 4–7 percent (depending on the concentration of H_2O in the melt).

All experiments were carried out in solid-media, high-pressure apparatus (Boyd and England, 1960) using the piston-out technique with a −4 percent correction for friction (calibrated against the quartz–coesite transition). The temperatures were measured with Pt–Pt90Rh10 thermocouples. The uncertainties were ±1 kbar and ±6°–10°C (Eggler, 1977; Mao *et al.*, 1971).

The Raman spectra were taken on small chips of quenched melt (about 0.5–1.0 mm cubes) free of bubbles. The spectra were recorded with a Jobin-Yvon optical system, holographic grating, double monochromator (HG25) with a photon-counting detection system. The spectra were recorded at 3 cm^{-1}/sec. The samples were excited with the 488.0 nm line of an Ar^+ laser using laser power of 200–400 mW at the sample with 90° scattering geometry. Polarized spectra were obtained with the focused exciting beam parallel to the horizontal spectrometer slit and with the electric vector of the exciting radiation in a vertical orientation. A sheet of polarizer disk in front of an optical scrambler was used to record separately the parallel and perpendicular components of the scattered radiation.

Several of the high-frequency envelopes of the

[2] NBO/T denotes nonbridging oxygen per tetrahedral cation. The tetrahedral cation can be Si^{4+}, Ti^{4+}, P^{5+}, Al^{3+}, and Fe^{3+}. With Fe^{3+} and Al^{3+}, local charge balance is attained with an alkali metal or an alkaline earth to form complexes such as $MAlO_2$, $MFeO_2$ and MAl_2O_4. MFe_2O_4 complexes are not stable in silicate melts (Mysen *et al.*, 1979a). The notation NBO/Si is used when T = Si.

Table 1. Raman spectroscopic data on the system Na_2O–SiO_2–D_2O–H_2O at 1300°C and 20 kbar

Composition	Mole % H_2O (D_2O)	Wavenumber, cm^{-1}							$\frac{I(1100)}{I(1060)}$	$\frac{I(1100)}{I(950)}$
$Na_2Si_2O_5$	...	573s,p	763w,p	948m,p	...	1055m,p	1103s,p	...	4.52	3.47
$Na_2Si_2O_5$	33.6 (D_2O)	573s,p	770w,p	943w,p(bd)	...	1057s,p	1098s,p	...	2.12	4.10
$Na_2Si_2O_5$	8.1	579s,p	764w,p	939mw,p	983w	1061s,p	1098s,p	...	1.61	4.19
$Na_2Si_2O_5$	14.4	574s,p	767w,p	940w,p(bd)	983w(bd)	1070s,p	1100s,p	...	1.11	3.64
$Na_2Si_3O_7$	...	542s,p	775w,p	942w,p	...	1065m,p	1093s,p	...	0.81	...
$Na_2Si_3O_7$	44.8 (D_2O)	538s,p	780w,p	...	...	1050s,p(bd)	1097s,p	1152m,p	3.89	...
$Na_2Si_3O_7$	8.6	539s,p	777w,p	...	972w(bd)	1061m,p(bd)	1101s,p	1173w(bd)	1.82	...
$Na_2Si_3O_7$	24.3	546s,p	773w,p	...	978m,p	1056s,p	1093s,p	1152m,p	0.96	...
$Na_2Si_3O_7$	37.9	546s,p	773w,p	...	973m	1062s,p	1093s,p	1147m,p	0.81	...

Abbreviations: s, strong; m, medium; mw, medium to weak; w, weak; vw, very weak; (bd), broad; (sh), shoulder; p. polarized. Band positions above 1200 cm^{-1} not accurately measured. For detailed positions of such bands (HOH and DOD stretch bands), see Table 2.

spectra were attempted deconvoluted into individual peaks. The details of the procedures used are described by Mysen *et al.* (1980).

Results

Volatile-free melts

The structural interpretation of volatile-free, quenched NS2 and NS3 melts at 1 atm and at high pressure has been presented elsewhere (Brawer and White, 1975; Furukawa and White, 1980; Mysen *et al.*, 1980). Only a summary of the band positions (Table 1) and interpretation of the Raman spectra are given here. The Raman spectrum of quenched NS2 melt consists of three polarized bands that are important for the present discussion. The strong band near 1100 cm^{-1} is due to ^-O–Si–O^0 stretching[3] (diagnostic of sheet units in the melt). The band near 950 cm^{-1} is due to ^-O–Si–O^- stretching (diagnostic of chain units), and that near 1060 cm^{-1} is due to Si–O^0 stretching (three-dimensional network unit). Other bands near 570 and 770 cm^{-1}, respectively, are due to Si–O^0 rocking and bending motions.

In volatile-free melt of $Na_2Si_2O_5$ composition, the following expression can be used to describe the equilibrium between the anionic structural units of the melt (Mysen *et al.*, 1980):

$$2Si_2O_5^{2-}\ (\text{sheet}) = Si_2O_6^{4-}\ (\text{chain}) + SiO_2\ (3D) \quad (1)$$

The same bands occur in volatile-free, quenched NS3 melt as in volatile-free NS2 melt (Table 1). Mysen *et al.* (1980) concluded, therefore, that quenched NS2 and NS3 melts contain the same structural units and that the equilibrium expressed with equation 1 applies to both melt compositions. The two melts differ, however, in that chain units are more dominant in NS2 than in NS3 melts, as indicated by the intensity ratios of diagnostic bands.

Virgo *et al.* (1980) found that analogous expressions could be derived for binary melts with greater NBO/Si than NS2. In those cases, the expressions were :

for NBO/Si between 1.0 and 2.0:

$$3Si_2O_6^{4-}\ (\text{chain}) = 2Si_2O_4^{2-}\ (\text{sheet}) + 2SiO_4^{4-}\ (\text{monomer}) \quad (2)$$

and for NBO/Si between 4.0 and 2.0:

$$2Si_2O_7^{6-}\ (\text{dimer}) = Si_2O_6^{4-}\ (\text{chain}) + 2SiO_4^{4-}\ (\text{monomer}) \quad (3)$$

Mysen *et al.* (1980) noted that the same expressions hold true regardless of the type of network-modifying cation. They also concluded that this structural model does not agree with models based on polymer theory, and presented arguments as to why this would be expected. This model is, however, consistent with rheological data on silicate melts (Bockris *et al.*, 1956). The interested reader is referred to Mysen *et al.* (1980) for a complete discussion of the present and other models.

The distinct assignments to monomers, dimers, chain, and sheets were also discussed in some length by Mysen *et al.* (1980), and no further discussion of those assignments is presented here.

The anionic structures of the two melts with three-dimensional network structure at 20 kbar (Jd and Ab melt) are also known (Virgo *et al.*, 1979a; Mysen *et al.*, 1980). Only band positions of volatile-free,

[3] O^{2-}, O^-, and O^0 denote free oxygen, nonbridging, and bridging oxygens, respectively. The notation Si–O^0 indicates that the vibration is from a bridging oxygen bond. In ^-O–Si–O^0, one oxygen (out of four) is nonbridging. In ^-O–Si–O^-, two oxygens per silicon are nonbridging.

Table 2. Band positions of Raman spectra from quenched melts in the system Na_2O–Al_2O_3–SiO_2–D_2O–H_2O at 1500°C and 20 kbar

Composition	Mole % H_2O (D_2O)	Wavenumber, cm^{-1}										$\frac{I(1100)}{I(870)}$	$\frac{I(1100)}{I(970)}$	$\frac{I(1100)}{I(1000)}$
$NaAlSi_2O_6$	...	470s,p	566w,p	784w,p	...	...	950m,p	1062s,p	...	2175s	2300w	...	...	...	...	2.17
$NaAlSi_2O_6$	27.4	480s,p	570p(sh)	773w,p	871w,dp	983w(bd)	966m,p	1058s,p	...*	...*	...*	...	...*	12.28	...	2.30
$NaAlSi_2O_6$	40.0	484s,p	561p(sh)	770w,p	862w,dp	985w(bd)	961m,p	1068s,p	...*	2180s	2300w	...	...*	8.34	10.[illegible]	2.42
$NaAlSi_2O_6$	51.9	484s,p	563p(sh)	770w,p	860w,dp	985w(bd)	940m,p	1062s,p	...*	...*	...*	...	...*	3.18	6.3[illegible]	2.63
$NaAlSi_3O_8$	...	468s,p	573w,p	794w,p	...	...	1000m,p	1100s,p	...	2175s	2300w	...	...	...	...	0.72
$NaAlSi_3O_8$	40.9 (D_2O)	465s,p	579p(sh)	806w,p	886w,dp	...	1000m,p	1100s,p	...	...*	...*	2583s(bd)	3566s(bd)	1.63	...	2.27
$NaAlSi_3O_8$	15.5	472s,p	573p(sh)	776w,p	874w,dp	976vw(bd)	1004m,p	1100s,p	...*	...*	...*	...	...*	16.7	10.8	1.23
$NaAlSi_3O_8$	27.5	476s,p	569p(sh)	790w,p	885w,dp	983w(bd)	1000m,p	1100s,p	1368w(bd)	...*	...*	...	3535s(bd)	3.6	8.0	1.37
$NaAlSi_3O_8$	38.9	484s,p	570p(sh)	785w,p	893w,dp	983mw(bd)	1000m,p	1100s,p	1374w(bd)	...*	...*	...	3530s(bd)	3.6	7.4	1.51

Abbreviations and uncertainties as in Table 1.
**Present but not determined accurately.*

quenched Jd and Ab melts are given (Table 2). Briefly, the high-frequency envelope consists of two (Si,Al)–O^0 stretch bands. Their frequencies are lowered with increasing Al content of the melt. The two stretch bands reflect two different three-dimensional network units in the melt. According to Mysen *et al.* (1980), these two units differ in average Si/(Si + Al), where the lowest frequency band is due to the most Si-rich unit. In addition, the Raman spectra show bands near 800, 570, and 470 cm^{-1}, which are due to Si–O^0 bending, decoupled defects, and Si–O^0 rocking, respectively (Bates *et al.*, 1974; Stolen and Walrafen, 1976). The three bands at these positions are diagnostic of the presence of three-dimensional network units in the quenched melts (Virgo *et al.*, 1979a).

In addition, the Raman spectra of all the samples, whether volatile-free or volatile-bearing, show two sharp bands near 2300 and 2200 cm^{-1}, respectively (Fig. 1). These two bands are due to N_2 and N_2^+ (Hartwig, 1977; Nakamoto, 1978) from air, and are

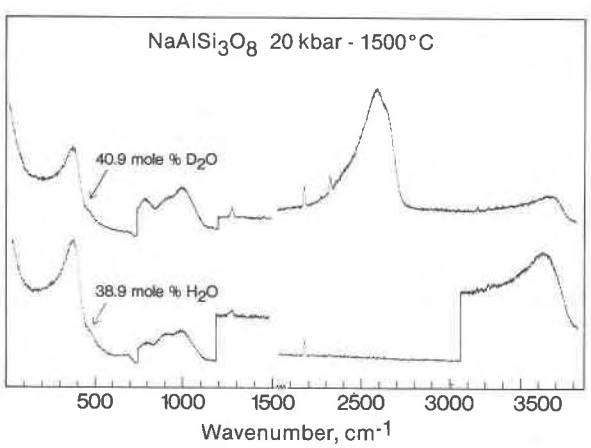

Fig. 1. Raman spectra (unpolarized) of quenched Ab + H_2O and Ab + D_2O melt.

of no consequence for the interpretation of the spectroscopic features under consideration. This observation is important because these two bands occur in the frequency region of Si–H stretching and could be misinterpreted as a result of such bonds. The two bands do not shift their frequency with composition, however, as would be expected if they were due to Si–H stretching (Lucovsky, 1979; Lucovsky *et al.*, 1979). Furthermore, no Si–H bands could be detected in the frequency region between 800 and 900 cm^{-1}.

Silicate melts with H_2O

Before the spectra of H_2O-bearing silicate melts are discussed, it is instructive to discuss the D_2O-bearing samples, because Si–OH stretch vibrations are expected in the frequency region near 950 cm^{-1} (Stolen and Walrafen, 1976). The Si–O stretch vibrations also occur in this frequency region. The analogous Si–OD bands are at frequencies that are lower than those of the OH vibrations by a factor of $\sqrt{2}$ (Van der Steen and Van den Boom, 1977; Hartwig, 1977).

The Raman spectrum of quenched Ab melt with 40.9 mole percent D_2O (calculated on the basis of 8 oxygens) is shown in Figure 1. The high-frequency envelope of this spectrum is compared with that of volatile-free and H_2O-bearing Ab melt in Figure 2. Detailed band positions are given in Table 2. The strong, broad, and asymmetric band near 2600 cm^{-1} is due to D–O–D stretching (Van der Steen and Van den Boom, 1977). The two sharp bands on the low-frequency shoulder of the 2600 cm^{-1} band are due to N_2 and N_2^+ from the air (see above). There is also a weak band near 3570 cm^{-1}, which is due to H–O–H stretching (*e.g.*, Stolen and Walrafen, 1976). This band is expected because the D_2O also contained about 5 percent H_2O.

Several changes have occurred in the high-fre-

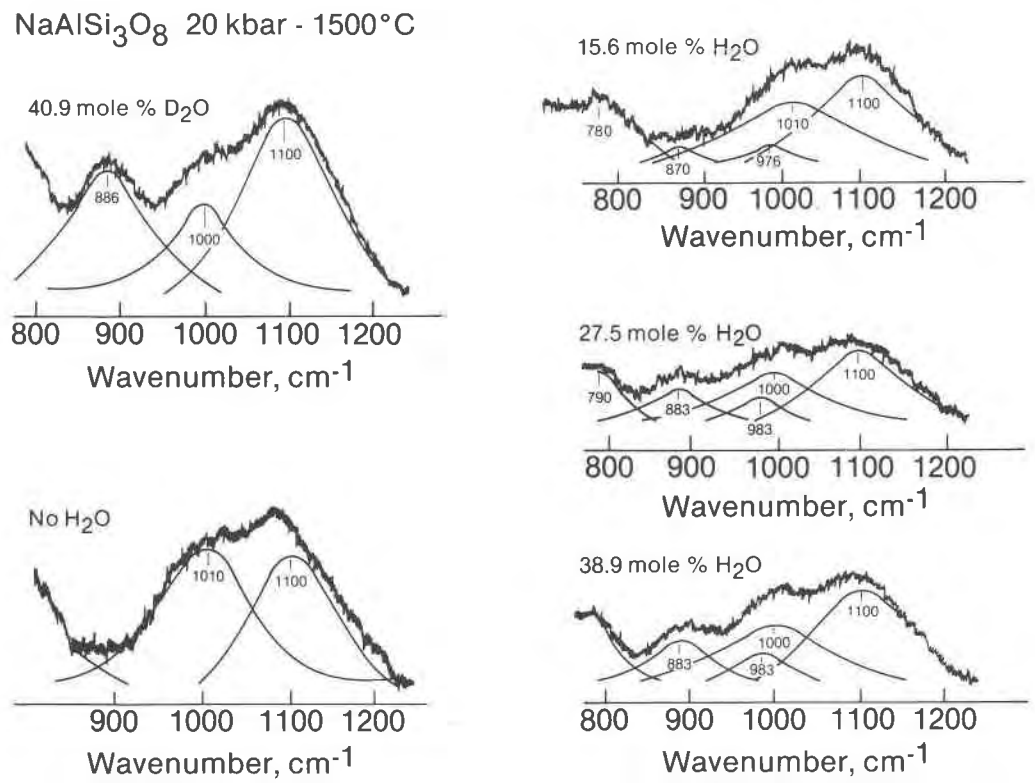

Fig. 2. High-frequency envelope of Raman spectra (unpolarized) of quenched Ab melt as a function of volatile content.

quency envelope of the spectrum from Ab + D_2O compared with the envelope of volatile-free Ab melt (Figs. 1 and 2). The two (Si,Al)–O^0 stretch bands remain in the same positions (about 1000 and 1100 cm^{-1}) as for the volatile-free melt. The intensity of the band near 1000 cm^{-1} is considerably weakened, however, relative to the 1100 cm^{-1} band [I(1100)/I(1000) is about 2.3 compared with 0.7 for volatile-free Ab melt; see also Table 2]. We conclude, therefore, that the proportion of Si-rich, three-dimensional network unit (3D) in Ab melt has been substantially reduced as a result of dissolved D_2O. It is emphasized, however, that the average Si/(Si + Al) of the two three-dimensional units is the same. Only the proportion of the Si-rich unit has been reduced.

A new band at 886 cm^{-1} occurs in deuterated, quenched Ab melt at 20 kbar and 1500°C (Fig. 2, Table 2). The D_2O contains only a very small amount of H_2O and the position and intensity of the 886 cm^{-1} band do not change appreciably whether 40 mole percent H_2O or 40 mole percent D_2O (with 5 percent H_2O) has been dissolved in the melt. It is not likely, therefore, that this band is due to vibrations involving D, H, OH, or OD-groups, as their intensities and frequencies would depend on concentration and type of volatile component added to the melt. We conclude, therefore, that the 880 cm^{-1} band cannot be assigned to Si–H, Si–D, Al–H, Al–D, Si–OH, Si–OD, Al–OH, or Al–OD vibrations. In addition, there are other arguments in favor of another interpretation. The Al–H, Al–D, Si–H, and Si–D vibrations may have bands that occur in the frequency range between 700 and 900 cm^{-1} (*e.g.*, Ryskin, 1974; Hartwig, 1977; Lucovsky, 1979; Lucovsky *et al.*, 1979; Peri, 1966). The band near 880 cm^{-1} could be due to Al–O^0, $^-$O–(Si,Al)–O^0 or $^-$O–(Si,Al)–O^- stretching. If it were due to Al–O^0 stretch vibrations, clusters of AlO_4 tetrahedra without nonbridging oxygens would be expected in the melt. This hypothesis is ruled out for the following reasons. In vibrational spectra known to contain AlO_4 clusters, Al–O^0 stretch vibrations result in one or more bands at 800 cm^{-1} or lower frequency (Tarte, 1967; Serna *et al.*, 1977, 1979; Virgo and Seifert, unpublished data, 1979), and no such bands are found in the hydrated samples. It is not likely, therefore, that the 880 cm^{-1} band found in the Ab + D_2O spectrum results from AlO_4 clusters. The band between 750 and 800 cm^{-1} found in the spectra of quenched Ab and Jd melts (Table 2) also

occurs at this frequency in Al-free melts with three-dimensional network units. The band in the deuterated and hydrated melts is not significantly affected by D_2O or H_2O content. This band is assigned to Si–O^0 bending, as also suggested by Bates *et al.* (1974) for quenched SiO_2 melt. No new bands occur in the spectral region below 800 cm^{-1} as a result of added volatiles. The presence of AlO_4 clusters is therefore ruled out.

The 880 cm^{-1} band changes its frequency with H_2O and Al content (Table 2) and hence is most likely a coupled (Si,Al) vibration. The intensity of the band relative to the (Si,Al)–O^0 stretch bands is so large, however, that it is unlikely that the 880 cm^{-1} band reflects vibrations of a bridging oxygen (see also Furukawa and White, 1980, for further discussion of such intensity considerations).

The 880 cm^{-1} band is polarized and thus is probably a symmetric $^-$O–(Si,Al)–O^- stretch vibration rather than an asymmetric $^-$O–(Si,Al)–O^0 stretch vibration. Mysen and Virgo (1979) noted that in quenched melts of $NaCaAlSi_2O_7$ composition [Si/(Si + Al) = 0.33 as compared with 0.25 in $NaAlSi_3O_8$ composition] the $^-$O–Si–O^- stretch band found near 950 cm^{-1} was shifted to near 900 cm^{-1} as a result of (Si,Al) coupling. In the system $NaAlSi_3O_8 + D_2O$, the average Si/(Si + Al) is greater than in $NaCaAlSi_2O_7$. As discussed further below, the Si/(Si + Al) of the anhydrous portion of the melt is less than this average value, however, because some of the Si of the melt is no longer part of the anhydrous network (owing to the formation of Si–OH- or Si–OD-containing structural units in the melt). The Si–OD band (stretch) is expected near 600 cm^{-1}. This is a weak band, however (Stolen and Walrafen, 1976; Van der Steen and Van den Boom, 1977), and is unresolved beneath the asymmetric band with a maximum near 500 cm^{-1} (Fig. 2). As a result of these considerations, we conclude that the 880 cm^{-1} band in quenched Ab + D_2O melt is due to symmetric $^-$O–(Si,Al)–O^- stretching. The (Si,Al) coupling is more extensive than indicated by the average Si/(Si + Al) of the melt. This band is, therefore, diagnostic of anhydrous (or undeuterated) chain units in the quenched Ab melt with 40.9 mole percent D_2O in solution.

The Raman spectra of quenched Ab + H_2O melt are shown in Figures 1 and 2, and band positions are given in Table 2. All spectra show the same features as the spectrum for Ab + D_2O, except that the H–O–H and Si–OH vibrations occur at different frequencies because of the different mass of H compared with D (Van der Steen and Van den Boom, 1977). A broad, asymmetric band near 3520 cm^{-1} is assigned to H–O–H stretching (Stolen and Walrafen, 1976). The asymmetry toward lower frequency is probably due to weak OH···O hydrogen bonds (Serratosa and Vinas, 1964; Peri, 1966). Hydrogen bonds between outer hydroxyl groups and neighboring oxygen are frequently observed in micas, for example (Serna *et al.*, 1977, 1979).

There are no bands at higher frequency than the H–O–H band; thus the presence of molecular H_2 in the quenched Ab + H_2O melt is ruled out (Lucovsky *et al.*, 1979). The absence of a band near 1600 cm^{-1} rules out the possibility of a contribution of molecular H_2O in solution in any of these melts (Lucovsky *et al.*, 1979). The two sharp bands near 2200 and 2300 cm^{-1} are due to N_2^+ and N_2 from the air (see also above). The weak band near 1380 cm^{-1} (Fig. 2) is due to H–O–H bending (Ryskin, 1974).

We note that the intensity of the band near 570 cm^{-1} [due to defects (broken oxygen bridges) in the three-dimensional network structure (Bates *et al.*, 1974; Stolen and Walrafen, 1976)] is lower in the spectra of melts with H_2O (and D_2O) than in those of melts without volatiles (Fig. 3). Stolen and Walrafen (1976) made similar observations in the system SiO_2–H_2O. They concluded that H^+ reacted with defects in the three-dimensional network structure (Si–O^-···Si–O–Si^-) to form OH, thereby diminishing the intensity of this band. The same mechanism explains the reduced intensity of the 570 cm^{-1} band in the spectra shown here. Stolen and Walrafen (1976) noted, however, that only about 1000 ppm H_2O can dissolve in fused SiO_2 according to this mechanism, and it is

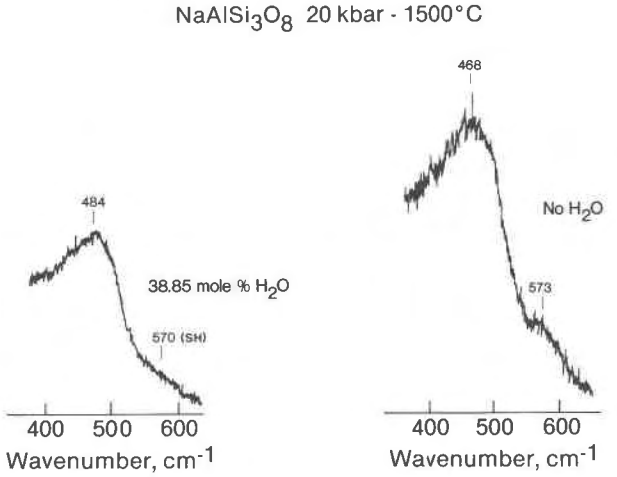

Fig. 3. Low-frequency region of volatile-free and H_2O-bearing quenched Ab melt.

therefore not considered the major mechanism for solution of several weight percent H_2O.

The band near 880 cm^{-1} in quenched Ab + D_2O melt also occurs in quenched Ab + H_2O melt (Fig. 2) and is at nearly the same position (within experimental uncertainty).

The 1000 cm^{-1} shoulder in Ab + H_2O spectra is stronger than in the spectrum from Ab + D_2O (Fig. 2). This higher intensity is caused by the presence of two bands in the frequency region near 1000 cm^{-1}. One is due to (Si,Al)–O^0 stretching from the silica-rich, three-dimensional network unit (1000 cm^{-1}). The other band (near 980 cm^{-1}) is an Si–OH stretch vibration. It may be argued that the 980 cm^{-1} band may also be due to Al–OH stretching. This possibility is considered unlikely because (1) the band occurs at the same frequency in Al-free samples (*e.g.*, Stolen and Walrafen, 1976; see also below) and (2) several Al–OH bending and rocking vibrations would be expected in the frequency region between 950 and 750 cm^{-1} (Ryskin, 1974). No such bands were found in our samples.

The 880 cm^{-1} band may shift to slightly higher frequency with increasing water content of quenched Ab melt (Fig. 4). The frequencies of the 1000 and 1100 cm^{-1} bands are not affected by the presence of water in the melt. The frequency increase of the 880 cm^{-1} band with increasing water content indicates that the average Si/(Si +Al) of this structural unit in quenched Ab melt increases slightly with increasing H_2O content.

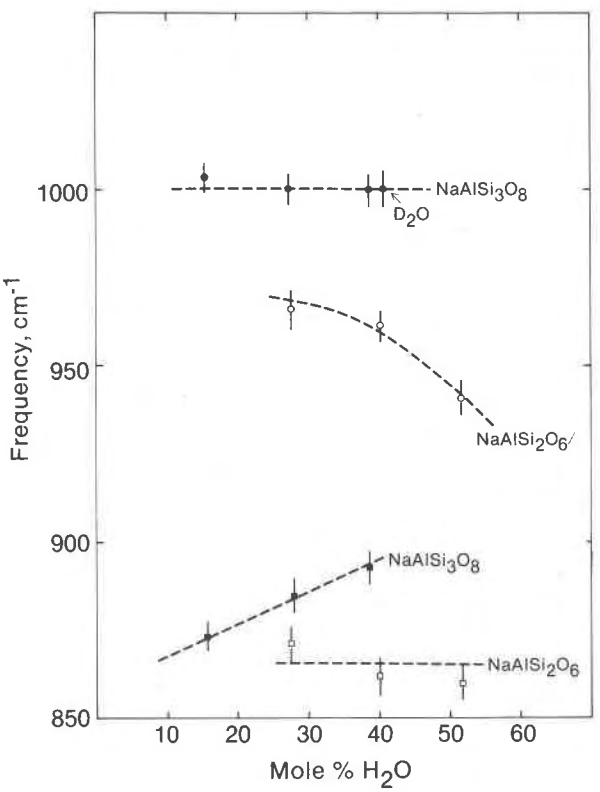

Fig. 4. Frequency shifts of critical Raman bands as a function of water content.

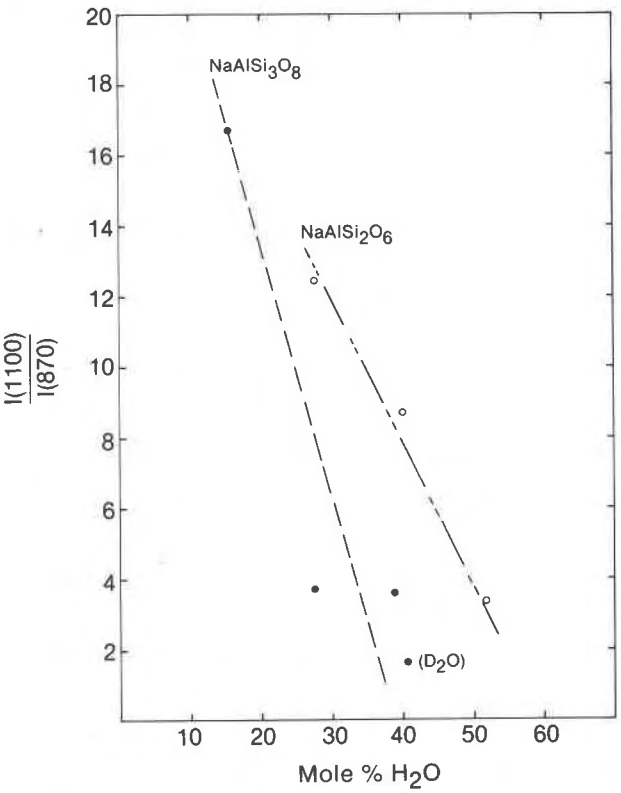

Fig. 5. Raman band intensity ratios $I(1100)/I(870)$, of volatile-free and volatile-bearing quenched Ab and Jd melts.

The intensities of both the 880 and 980 cm^{-1} bands increase relative to those of the 1100 and 1000 cm^{-1} (Al,Si)–O^0 stretch bands as the water content of the Ab melt is increased (Fig. 5; see also Table 2). We conclude, therefore, that more chain units and Si–OH bands are formed as the water content of the melt is increased. Finally, the intensity ratio, $I(1100)/I(1000)$, increases with increasing water content (Fig. 6). This increase implies that the Si–OH groups are formed as a result of interaction between the H_2O and the most silica-rich of the two three-dimensional network units in melt of $NaAlSi_3O_8$ composition.

The high-frequency envelope of the Raman spectra of quenched melts of $NaAlSi_2O_6$ and $NaAlSi_2O_6 + H_2O$ composition are shown in Figure 7 (see also Table 2). The portions of these spectra at higher

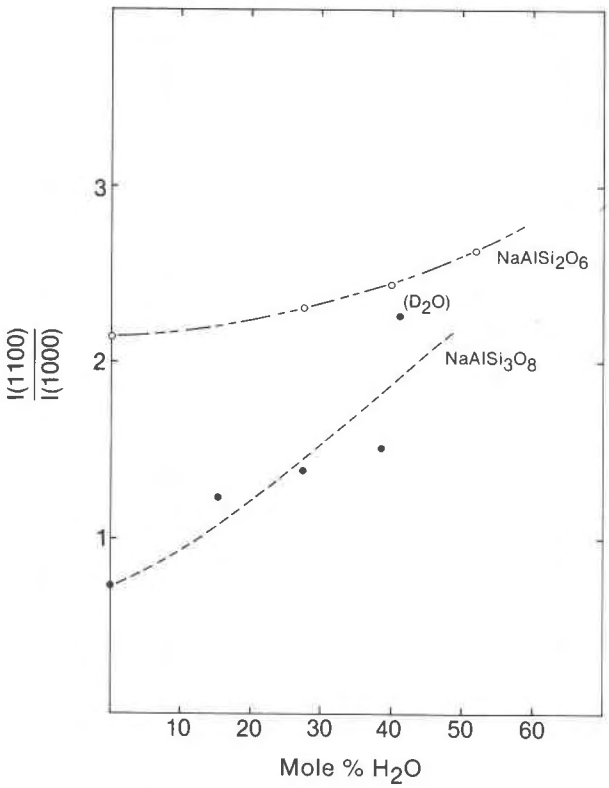

Fig. 6. Raman band intensity ratios, $I(1100)/I(1000)$, of volatile-free and volatile-bearing quenched Ab and Jd melts.

and lower frequencies than those shown in Figure 7 are identical with the same regions in the spectra of quenched Ab + H_2O melt and are not included. The exact band positions from these regions are given in Table 2.

The structure of quenched anhydrous Jd melt at high pressure has been described by Mysen *et al.* (1980). Briefly, the structure closely resembles that of quenched anhydrous Ab melt except that the two three-dimensional network units are more Al-rich in the Jd than in the Ab melt. The proportion of the most Si-rich unit relative to the Al-rich unit is also smaller in Jd melt.

Addition of water to Jd melt results in the same changes in the high-frequency envelope of the Raman spectra of both Ab and Jd melts (Figs. 2 and 7). A new, polarized band occurs near 860 cm^{-1}. This band is analogous to the 880 cm^{-1} band in quenched Ab + H_2O melt and is assigned to symmetric ^-O–(Al,Si)–O^- stretching, as in quenched Ab + H_2O melt. Its slightly lower frequency in Jd + H_2O melt is a result of the smaller Si/(Si + Al) of Jd compared with Ab melt. The intensity of this band relative to the (Si,Al)–O^0 stretch bands increases with increasing water content of the melt, as was also the case for Ab + H_2O melt (Fig. 5). A new band near 980 cm^{-1} is assigned to Si–OH stretching. This band most likely does not reflect Al–OH stretching, for the same reasons as outlined above for Ab + H_2O melt. Finally, the intensity ratio, $I(1060)/I(950)$, increases with increasing water content (Fig. 6). This intensity increase corresponds to the intensity increase of $I(1100)/I(1000)$ for Ab + H_2O melt, and is interpreted to mean that the proportion of the Si-rich, three-dimensional network unit decreases relative to the Al-rich unit as the water content of quenched Jd melt is increased.

In summary, solution of H_2O in melts of $NaAlSi_3O_8$ and $NaAlSi_2O_6$ has similar effects on the anionic structure of the melts. First, water is bound in the structure as Si–OH, resulting in a decrease in the average Si/(Si + Al) of the anhydrous portion of the melt. The three-dimensional network portion of the melt responds to this decrease by an increase in the proportion of the Al-rich unit relative to the Si-rich, three-dimensional network unit. Second, (Si,Al)-coupled chains of the type $NaAlSiO_6^{4-}$ are formed. No OH groups are attached to the chain units. Third, aluminum is not attached to hydroxyl in any complex in the melt. Fourth, it is not possible to determine from the Raman spectra whether complexes involving Na^+ and OH^- occur in the melt. This unidentified complex is referred to as $Na(OH)^0$ in the remainder of the text.

A comparison of the high-frequency envelopes of the Raman spectra of quenched melts of $Na_2Si_3O_7$ and $Na_2Si_3O_7$ + 44.8 mole percent D_2O (based on the chemical formula—7 oxygens) is shown in Figure 8, and detailed data are given in Table 1. A comparison of the spectra of the volatile-free samples with the deuterated sample is conducted first, to avoid interferences from OH bands in the high-frequency envelope (see also above).

Three features are evident from the comparison of the volatile-free and the deuterated samples. First, the 940 cm^{-1} band diagnostic of chain units in anhydrous NS3 melt cannot be discerned in the deuterated sample. Second, a new band near 1150 cm^{-1} is observed in the Raman spectrum of quenched NS3 + D_2O. We suggest that this is the band found at 1200 cm^{-1} in quenched SiO_2 melt and assigned to Si–O^0 stretching (Bates *et al.*, 1974). Brawer and White (1975, 1977) noted that this band shifts from 1200 cm^{-1} to near 1150 cm^{-1} as Na_2O is added to SiO_2 melt on the join Na_2O–SiO_2. The band disappears at

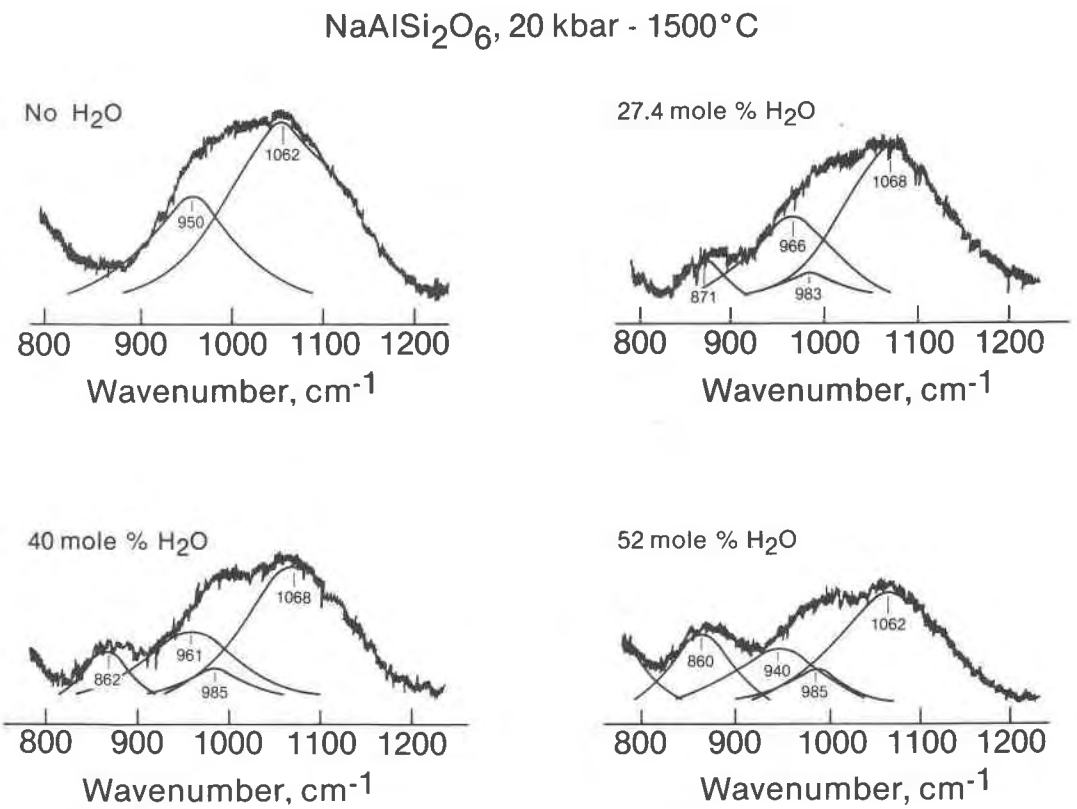

Fig. 7. High-frequency region of Raman spectra of volatile-free and volatile-bearing quenched Jd melt.

Na_2O/SiO_2 = 1/3–1/4. The reappearance of this band with the addition of D_2O to quenched melt of NS3 composition (Na_2O/SiO_2 = 1/3) indicates that the proportion of bridging oxygen is greater in deuterated than in volatile-free melt of NS3 composition. Third, the intensity of the 1100 cm^{-1} band (indicating that sheet units may be present in the melt; Mysen *et al.,* 1980) relative to the intensity of the 1050 cm^{-1} band (Si–O^0 antisymmetric stretch band; Furukawa and White, 1980; Mysen *et al.,* 1980) has decreased. This observation also implies that deuterated NS3 melt is more polymerized than D_2O-free, quenched melt of $Na_2Si_3O_7$ composition.

The high-frequency envelopes of the Raman spectra of hydrated quenched NS3 melt are shown in Figure 9 (see also Table 1). When curves were fitted to the high-frequency envelope (see Mysen *et al.,* 1980, for the fitting procedure), the bands near 1050, 1100, and 1150 cm^{-1} were retained. In order to fulfill this requirement, a broad band near 970 cm^{-1} also had to be included. This band becomes more intense with increasing water content, and because of this relation and its frequency, it is assigned to Si–OH stretching.

The intensity ratio of the 1100 and 1050 cm^{-1} bands is plotted as a function of H_2O content of the melt in Figure 10. These data show that the 1050 cm^{-1} band becomes more intense as the water content of the melt increases. This observation is interpreted to mean that the solution of H_2O in melt of $Na_2Si_3O_7$ composition results in the formation of Si–OH bonds with a concomitant decrease of NBO/Si of the melt.

The effect of dissolved H_2O and D_2O on the high-frequency envelope of the Raman spectra of quenched NS2 melt is shown in Figure 11. A comparison of the spectra of volatile-free, D_2O-bearing, and H_2O-bearing NS2 melt shows the same bands in all cases (940 cm^{-1}, $Si_2O_6^{4-}$ chains; 1060 cm^{-1}, SiO_2 three-dimensional network; 1100 cm^{-1}, $Si_2O_6^{2-}$ sheets). It is clear, however, that the intensity ratio $I(1100)/I(1060)$ has decreased and $I(1100)/I(940)$ has increased (Table 1; see also Fig. 10). As for hydrous melt of NS3 composition, these changes are interpreted to mean that the proportion of bridging oxygen in the melt has increased as water is dissolved. This change is reflected in an increased ratio of three-dimensional network units to sheet units, and an in-

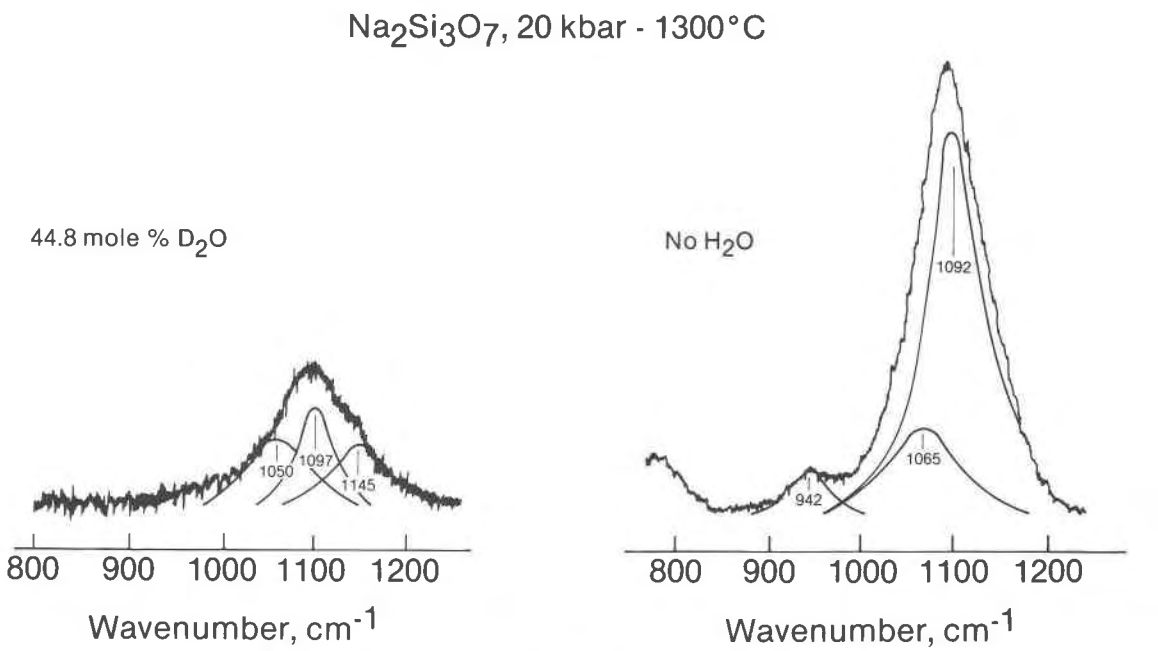

Fig. 8. High-frequency region of volatile-free and D_2O-bearing quenched melt of $Na_2Si_3O_7$ composition.

crease of sheet units relative to chain units in the melt.

Addition of H_2O to quenched NS2 melt results in an additional change of the high-frequency envelope. A new band occurs near 980 cm^{-1}, which is the Si–OH stretch band also found in all the other compositions.

In summary, the influence of dissolved water on the structure of melts in the system Na_2O–SiO_2 appears similar for all compositions studied. Water is attached to the network with Si–OH bonds, and the hydroxyl-free portion of the network has become more polymerized. As in the systems Ab + H_2O and Jd + H_2O, it cannot be determined from the Raman spectra whether $Na(OH)^0$ occurs in the melts; however, mass-balance considerations require its presence. This conclusion contrasts with that for the other two compositions, in which $Na(OH)^0$ does not occur.

Solubility mechanisms

Even though H_2O reacts with silicate melts to form Si–OH bonds, two distinctly different solubility mechanisms are necessary to explain the spectroscopic observations, depending on whether the silicate melt contains nonbridging oxygen. Most solubility models for H_2O have been based on studies of melts with a three-dimensional network structure, and this type of melt is considered first.

The Raman spectra of hydrous Jd and Ab melt show the existence of four structural units. First, there are units that involve only Si and OH. Whether Si–O–Si bonds also exist in these structural units cannot be discerned from the Raman spectra. Second, there are chain units without OH but with both Si and Al. The Al^{3+} must be locally charge-balanced with Na^+. The exact proportion of Si and Al in the chain unit cannot be determined. In the present discussion, the chain unit is described by the formula $NaAlSiO_6^{4-}$, where Al, therefore, is in tetrahedral coordination. Third, a portion of the three-dimensional network units is not affected by the presence of H_2O in the melt. The proportion of the latter two units and the OH/Si of the hydroxylated silicate unit depends on the H_2O content of the melt. Fourth, Burnham (1975) noted that the equimolal solubility of H_2O in $NaAlSi_3O_8$ melt is about 10 percent greater than in Si_4O_8. This additional water is dissolved as OH^-, locally charge-balanced by Na^+. This configuration in the melt is referred to as $Na(OH)^0$ in this text. This notation is not meant to imply that such complexes actually occur in the melt.

A consequence of the formation of chain units from a three-dimensional network structure is the expulsion of some Al^{3+} from tetrahedral coordination. There is no evidence that either this or any other Al^{3+} is coordinated with OH groups. An equivalent amount of Na^+ must also be transformed from its charge-balancing role to become a network modifier.

The extra Al^{3+} is referred to simply as Al^{3+} in the

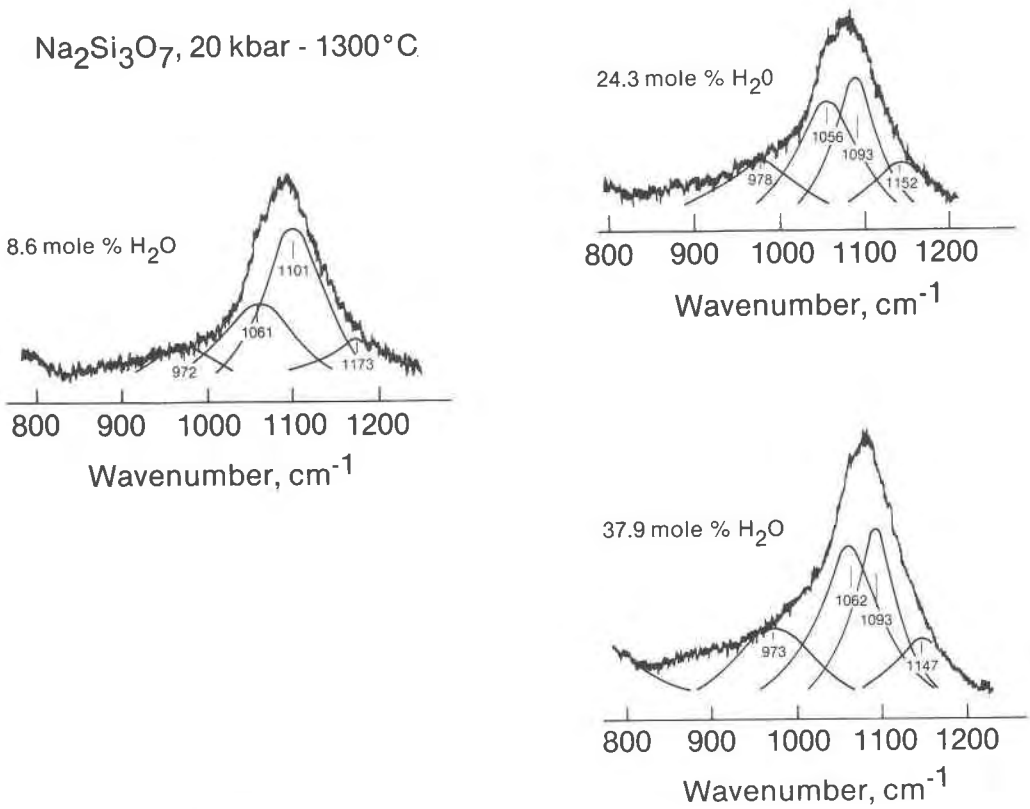

Fig. 9. High-frequency region of water-bearing, quenched melt of $Na_2Si_3O_7$ composition.

expressions below. This notation is meant to indicate the proportion of aluminum in the melt that is no longer in tetrahedral coordination. Instead, this proportion of the total amount of aluminum in the melt has become a network-modifier.

The formation of Si–OH bonds from bridging oxygen is visualized as follows:

$$\text{–Si–O–Si– (melt)} + H_2O\ \text{(vapor)} = \text{–Si–OH . . . HO–Si– (melt)} \quad (4)$$

The principle illustrated with this expression was also proposed by Kurkjian and Russell (1957), Wasserburg (1957), Adams and Douglas (1959), and Uys and King (1963). The formation of two OH groups per molecule of H_2O was indicated by the fact that the H_2O solubility was proportional to $[f(H_2O)]^{1/2}$ (Kurkjian and Russell, 1957).

In view of the above observations and discussion, an idealized expression that describes the solubility mechanism of H_2O in melt of $NaAlSi_3O_8$ composition can be written:

$$14NaAlSi_3O_8\ \text{(melt)} + 13xH_2O\ \text{(vapor)} = 9Si_4O_{8-x}(OH)_{2x}\ \text{(melt)} + 8Na(OH)^0\ \text{(melt)} + 8Al^{3+}\ \text{(melt)} = 6NaAlSiO_6^{4-} \quad (5)$$

The Al^{3+} in equation 5 reflects the proportion of aluminum that is now a network modifier. With x = 2, 4, 6, and 8, the hydroxylated silicate is respectively a sheet, chain, dimer, and monomer. The corresponding amount of H_2O that can be dissolved in Ab melt with these values for x is given in Table 3. The results of the latter calculations (Table 3) show that in our quenched melts the hydroxylation probably did not proceed beyond sheets $[Si_4O_6(OH)_4]$.

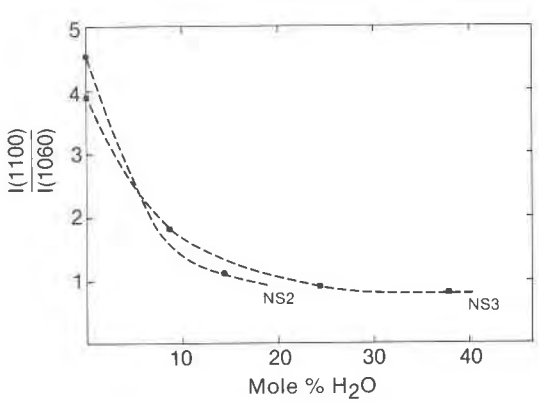

Fig. 10. Raman band intensity ratio, $I(1100)/I(1060)$, of quenched NS3 and NS2 melts as a function of water content.

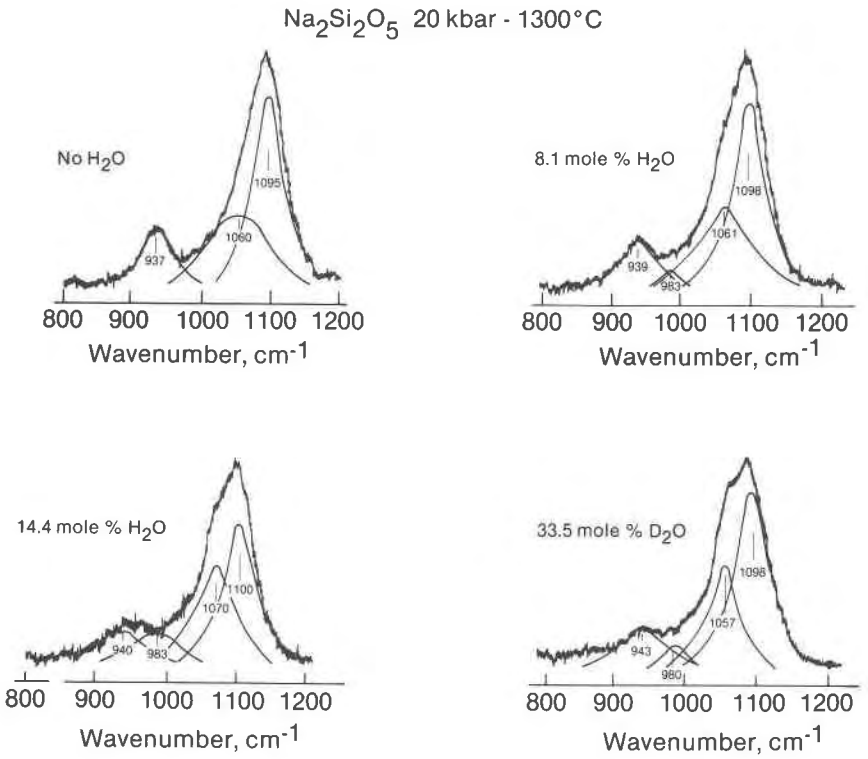

Fig. 11. High-frequency region of volatile-free and water-bearing quenched melt of $Na_2Si_2O_5$ composition.

The Raman spectra of quenched hydrated melt of $NaAlSi_2O_6$ composition indicate that the solubility mechanism for H_2O in such melts in similar to that in Ab melt. The analogous expression is

$$28NaAlSi_2O_6\ (melt) + 15xH_2O\ (vapor) = 11Si_4O_{8-x}(OH)_{2x}\ (melt) + 16Na(OH)^0\ (melt) + 16Al^{3+}\ (melt) + 12NaAlSiO_6^{4-}\ (melt) \quad (6)$$

The maximum solubilities of H_2O corresponding to x = 2, 4, 6, and 8 are shown in Table 3.

We suggest that analogous mechanisms control the solubility of H_2O in melts with three-dimensional network structures but with other melt modifiers (*e.g.*, K or alkaline earths) or amphoteric cations (*e.g.*, Fe^{3+}). The solubility mechanisms of H_2O in silicate melts with nonbridging oxygen indicate the formation of Si–OH bonds with a concomitant decrease in NBO/Si of the melt. The formation of an Si–OH bond from $Si–O^-$ indicates that one H^+ has taken the place of an Na^+. The Na^+ released can be neutralized by forming $Na(OH)^0$, a model also advanced by Kurkjian and Russell (1957) on the basis of solubility studies on $Na_2O–SiO_2$ melts. In fact, the formation of $Na(OH)^0$ complexes is a consequence of the spectroscopic observation that $SiO_2/Si_2O_5^{2-}$ increases with increasing water content of the melts.

Table 3. Maximum water solubility in silicate melts as a function of the number of OH groups attached to Si

Composition	Wt % H_2O			
	x=2 (sheet)	x=4 (chain)	x=6 (dimer)	x=8 (monomer)
$NaAlSi_3O_8$	9.7	17.8	24.5	30.2
$NaAlSi_2O_6$	8.2	15.2	21.1	26.3
$Na_2Si_3O_7$	11.0	19.9	27.1	33.2
$Na_2Si_2O_5$	14.2	24.8	33.1	39.7

The complete reactions for melts of $Na_2Si_3O_7$ and $Na_2Si_2O_5$ compositions may be written:

$$6Na_2Si_3O_7\ (melt) + 5xH_2O\ (vapor) = 2Si_4O_{8-x}\ (OH)_{2x}\ (melt) + 6SiO_2\ (melt) + 12Na(OH)^0\ (melt) \quad (7)$$

and

$$6Na_2Si_2O_5\ (melt) + 5xH_2O\ (vapor) = 2Si_4O_{8-x}\ (OH)_{2x}\ (melt) + 4SiO_2\ (melt) + 12Na(OH)^0\ (melt) \quad (8)$$

The maximum water solubilities for given values of x (Table 3) show that for given x the water solubility increases with increasing Na_2O/SiO_2, as also concluded by Uys and King (1963) on the basis of water solubility studies on melts on alkali–silica joins.

We suggest that solution mechanisms similar to those shown in equations 7 and 8 also operate in

metasilicate melts. In those melts, chain units are the predominant units, and the hydroxylated units can be no more polymerized than that.

In summary, the Raman spectra of quenched hydrated melts with a three-dimensional network structure show that nonbridging oxygens are formed in addition to hydroxylated silicate units. In melts with nonbridging oxygen, the Raman spectra show an increase in the degree of polymerization of the network. Water is bonded in the structure as both Si–OH and complexes of the type $M(OH)^0$, where M is a modifying cation.

Applications

Water affects the melting relations of silicate mineral assemblages. Kushiro (1969) has shown, for example, that in the system $CaO–MgO–SiO_2–H_2O$ the pyroxene–silicate mineral liquidus boundary shifts significantly toward the silica-rich portion of the system with the addition of H_2O. This observation is understandable in the light of the solubility mechanisms for water in highly polymerized melts where $X(T_2O_6)/(XTO_2)$ increases as a function of increasing water content of the melt.[4] If it is assumed that the relative changes of concentration of the structural units in the melt can be approximated with the relative changes of their activities (activity coefficient ratios are constant), the stability field of the most silica-rich mineral is reduced simply because $X(TO_2)/[X(TO_2) + X(T_2O_6)]$ has decreased.

The plagioclase stability field shrinks at the expense of pyroxene stability fields as H_2O is added to natural and synthetic andesite systems (*e.g.*, Kushiro, 1972; Eggler, 1972). These changes can also be directly related to the increased importance of T_2O_6 units in the melts with increasing water content.

Partial melts from hydrous peridotite in the upper mantle are more siliceous than those from anhydrous peridotite (*e.g.*, Kushiro *et al.*, 1972; Mysen and Boettcher, 1975). Carmichael *et al.* (1974) explained such observations by stating that the activity of silica in the hydrous partial melts is lower than in the anhydrous partial melts. The reason for this lowering of silica activity is the lowering of $X(TO_2)/[X(TO_2) + X(T_2O_6)]$ as water is added to the system.

Melt structure (bulk composition) affects crystal–liquid partition coefficients (Watson, 1976, 1977; Hart and Davis, 1978; Mysen *et al.*, 1979c). The most important feature of the melt structure affecting the partition coefficients is the ratio of nonbridging to bridging oxygen in the melt. The crystal–liquid partition coefficients of both transition metals and rare earth elements decrease with increasing NBO/T of the melt (Mysen *et al.*, 1979c). Solution of H_2O in highly polymerized melts (*e.g.*, basalt, andesite and granite) results in an increase of NBO/T. We suggest, therefore, that crystal–liquid partition coefficients will decrease with increasing water content. In melts with a large value of NBO/T (*e.g.*, picrite, komatiite, and basanite), it is likely that solution of H_2O results in decreased NBO/T. In such cases, the relevant crystal–liquid partition coefficients (*e.g.*, Ni between olivine and melt) will increase with increasing water content of the melt.

Iron is likely to play a similar role in silicate melts to aluminum (Seifert *et al.*, 1979). That is, in hydrous basaltic melts some ferric iron is a network modifier and some is a network former. The proportion of ferric iron in tetrahedral coordination will depend on the water content of the melt. The activity of ferric iron complexed in octahedral coordination in melts is greater than when ferric iron is in tetrahedral coordination (Seifert *et al.*, 1979; Mysen *et al.*, 1979b). Consequently, the stability fields of iron oxides on the liquidi of hydrous basalt differ from those of anhydrous basaltic melts not only because water affects the fugacity of hydrogen (*e.g.*, Osborn, 1959), but also because it affects the structural role of ferric iron in the melt.

Physical properties of silicate melts (*e.g.*, electrical conductivity and viscosity) depend on their water content (Lebedev and Khitarov, 1964; Shaw, 1963; Kushiro, 1978; Kushiro *et al.*, 1976). In anhydrous melts of basaltic and more acidic composition, NBO/T is less than 1 (Bottinga and Weill, 1972; Scarfe *et al.*, 1979; Mysen *et al.*, 1979a). In such melts, the flow units during viscous flow are SiO_2-rich, three-dimensional clusters (Mysen *et al.*, 1979a). The clusters are bonded with T–O bonds, where the T cation is tetrahedrally coordinated Al^{3+}, Ti^{4+}, and Fe^{3+}. The viscosity of such melts depends on the strength of the T–O bond (*e.g.*, Taylor and Rindone, 1970). In melts with NBO/T > 1, the flow units are isolated SiO_4 tetrahedra and modifying cations (*e.g.*, Bockris *et al.*, 1955). The viscosity of such melts depends on the number of oxygen bridges that must be broken to form the flow units. Furthermore, only a portion of the melt participates in the viscous flow at any given time. In this case, the viscosity of a melt with a sheet structure, for example, is greater than that of one

[4] The notations $X(TO_2)$, $X(T_2O_5)$ and $X(T_2O_6)$, respectively, denote proportions of melt units with a three-dimensional network, sheet, and chain structure. The T cation can be Si^{4+}, Ti^{4+}, P^{5+}, $(NaAl)^{4+}$, $(½CaAl)^{4+}$, and $(NaFe)^{4+}$.

with a chain structure, and so on. The viscosity of such melts is also lower than in melts with three-dimensional network structure because of the smaller size of the flow units. We suggest that viscous flow of hydrous basaltic and more silica-rich melts is controlled by the latter mechanism, whereas in the anhydrous equivalents the viscous flow is controlled by the former mechanism. Hence hydrous melts are more fluid than anhydrous, highly polymerized melts.

We may also speculate that because H_2O in effect increases NBO/T in less polymerized melts, the viscosity of melts of picrite, komatiite, and basanite composition may increase as a result of the dissolution of water.

Acknowledgments

Critical reviews by D. H. Eggler, E. Takahashi, W. B. White, and H. S. Yoder, Jr. are appreciated. Scarfe acknowledges support from the Carnegie Institution of Washington and Canadian NSERC grant A 8394. This research was partially supported by NSF grant EAR 7911313 and partially by the Carnegie Institution of Washington.

References

Adams, R. V. and R. W. Douglas (1959) Infrared studies on various samples of fused silica with special reference to the bands due to water. *J. Soc. Glass Technol., 42,* 147–158.

Bates, J. B., R. W. Hendricks and L. B. Shaffer (1974) Neutron irradiation effects and structure of non-crystalline SiO_2. *J. Chem. Phys., 61,* 4163–4176.

Bockris, J. O'M., J. D. MacKenzie and J. A. Kitchner (1955) Viscous flow in silica and binary liquid silicates. *Trans. Faraday Soc., 51,* 1734–1748.

Bottinga, Y. and D. F. Weill (1972) The viscosity of magmatic silicate liquids: a model for calculation. *Am. J. Sci., 272,* 438–475.

Boyd, F. R. and J. L. England (1960) Apparatus for phase equilibrium measurements at pressures up to 50 kilobars and temperatures up to 1750°C. *J. Geophys. Res., 65,* 741–749.

Brawer, S. A. and W. B. White (1975) Raman spectroscopic investigation of the structure of silicate glasses. I. The binary silicate glasses. *J. Chem. Phys., 63,* 2421–2432.

——— and ——— (1977) Raman spectroscopic investigation of the structure of silicate glasses. II. Soda–alkaline earth–alumina ternary and quaternary glasses. *J. Non-Cryst. Solids, 23,* 261–278.

Burnham, C. W. (1974) $NaAlSi_3O_8$–H_2O solutions: a thermodynamic model for hydrous magmas. *Bull. Soc. fr. Mineral. Cristallogr., 97,* 223–230.

——— (1975) Thermodynamics of melting in experimental silicate–volatile systems. *Geochim. Cosmochim. Acta, 39,* 1077–1084.

——— and N. F. Davis (1971) The role of H_2O in silicate melts. I. *P-V-T* relations in the system $NaAlSi_3O_8$–H_2O to 10 kilobars and 1000°C. *Am. J. Sci., 271,* 54–79.

——— and ——— (1974) The role of H_2O in silicate melts. II. Thermodynamic and phase relations in the system $NaAlSi_3O_8$–H_2O to 10 kilobars, 700° to 1100°C. *Am. J. Sci., 274,* 902–940.

——— and R. H. Jahns (1962) A method for determining the solubility of water in silicate melts. *Am. J. Sci., 260,* 721–745.

Carmichael, I. S. E., F. J. Turner and J. Verhoogen (1974) *Igneous Petrology.* McGraw-Hill, New York.

Drake, M. J. and J. R. Holloway (1977) Partitioning of samarium between plagioclase, clinopyroxene, amphibole and hydrous silicate liquid at high pressure: preliminary results. In *Papers Presented at the International Conference on Experimental Trace Element Geochemistry, Sedona, Arizona,* 21–23.

Eggler, D. H. (1972) Water-saturated and water-undersaturated melting relations in a Parícutin andesite and an estimate of water contents in natural magma. *Contrib. Mineral. Petrol., 34,* 261–271.

——— (1977) Calibration of a Pyrex solid-media assembly. *Carnegie Inst. Wash. Year Book, 76,* 656–658.

——— and M. Rosenhauer (1978) Carbon dioxide in silicate melts. II. Solubilities of CO_2 and H_2O in $CaMgSi_2O_6$ (diopside) liquids and vapors at pressures to 40 kb. *Am. J. Sci., 278,* 64–94.

Furukawa, T. and W. B. White (1980) Raman spectroscopic investigation of the structure of silicate melts. III. Alkali–silico–germanates. *J. Chem. Phys.,* in press.

Goranson, R. W. (1931) The solubility of water in granitic magmas. *Am. J. Sci., 22,* 481–502.

Hamilton, D. L., C. W. Burnham and E. F. Osborn (1964) The solubility of water and effects of oxygen fugacity and water content on crystallization in mafic magmas. *J. Petrol., 5,* 21–39.

Hart, S. R. and K. E. Davis (1978) Nickel partitioning between olivine and silicate melt. *Earth Planet. Sci. Lett., 40,* 203–220.

Hartwig, C. M. (1977) The radiation-induced formation of hydrogen and deuterium compounds in silica as observed by Raman scattering. *J. Chem. Phys., 66,* 227–239.

Hodges, F. N. (1974) The solubility of H_2O in silicate melts. *Carnegie Inst. Wash. Year Book, 73,* 251–255.

Kennedy, G. C., G. J. Wasserburg, H. C. Heard and R. C. Newton (1962) The upper three-phase region in the system SiO_2–H_2O. *Am. J. Sci., 260,* 501–521.

Kurkjian, C. R. and L. E. Russell (1957) The solubility of water in molten alkali silicates. *J. Soc. Glass Technol., 41,* 130–144.

Kushiro, I. (1969) The system forsterite–diopside–silica with and without water at high pressures. *Am. J. Sci., 267A,* 269–294.

——— (1972) Effect of water on the composition of magmas formed at high pressures. *J. Petrol., 13,* 311–334.

——— (1978) Density and viscosity of hydrous calc-alkalic andesite magma at high pressure. *Carnegie Inst. Wash. Year Book, 77,* 675–678.

———, H. S. Yoder, Jr. and B. O. Mysen (1976) Viscosities of basalt and andesite melts at high pressures. *J. Geophys. Res., 81,* 6351–6356.

———, ——— and M. Nishikawa (1968) Effect of water on the melting of enstatite. *Geol. Soc. Am. Bull., 79,* 1685–1692.

———, N. Shimizu, Y. Nakamura and S. Akimoto (1972) Composition of coexisting liquid and solid phases formed upon melting of natural garnet and spinel lherzolites at high pressures: a preliminary report. *Earth Planet. Sci. Lett., 14,* 19–25.

Lebedev, E. E. and N. I. Khitarov (1964) The dependence of electrical conductivity of granite melt and the beginning of granite melting on high pressures of water. [in Russian] *Geokhimiya, 3,* 195–201.

Lucovsky, G. (1979) Chemical effects on the frequencies of Si–H vibrations in amorphous solids. *Solid State Commun., 29,* 571–576.

———, R. J. Nemanich and J. C. Knights (1979) Structural inter-

pretation of the vibrational spectra of α-Si:H alloys. *Phys. Rev. B, 19,* 2064–2073.

Mao, H. K., P. M. Bell and J. L. England (1971) Tensional errors and drift of thermocouple electromotive force in the single-stage, piston–cylinder apparatus. *Carnegie Inst. Wash. Year Book, 70,* 281–287.

Mysen, B. O. and A. L. Boettcher (1975) Melting of a hydrous mantle. II. Geochemistry of crystals and liquids formed by anatexis of mantle peridotite at high pressures and high temperatures as a function of controlled activities of water, hydrogen and carbon dioxide. *J. Petrol., 16,* 549–590.

———, D. Virgo and C. M. Scarfe (1980) Relations between the anionic structure and viscosity of silicate melts: a Raman spectroscopic study at 1 atmosphere and at high pressure. *Am. Mineral., 65,* 690–710.

———, ——— and F. Seifert (1979a) Melt structures and redox equilibria in the system CaO–MgO–FeO–Fe_2O_3–SiO_2. *Carnegie Inst. Wash. Year Book, 78,* 519–526.

———, ——— and ——— (1979b) Influence of melt structure on element partitioning between olivine and melt and between clinopyroxene and melt at 1 atm. *Carnegie Inst. Wash. Year Book, 78,* 542–547.

Nakamoto, K. (1978) *Infrared and Raman Spectra of Inorganic and Coordination Compounds,* 3d ed. Wiley, New York.

Orlova, G. P. (1964) The solubility of water in albite melts. *Int. Geol. Rev., 6,* 254–258.

Osborn, E. F. (1959) The role of oxygen pressure in the crystallization and differentiation of basaltic magma. *Am. J. Sci., 257,* 609–647.

Peri, J. B. (1966) Infrared study of OH and NH_2 groups on the surface of dry silica aerogel. *J. Phys. Chem., 70,* 2937–2945.

Ryskin, Ya. I. (1974) The vibrations of protons in minerals: hydroxyl, water and ammonium. In V. C. Farmer, Ed., *The Infrared Spectra of Minerals,* p. 137–183. Mineralogical Society, London.

Scarfe, C. M., B. O. Mysen and D. Virgo (1979) Changes in viscosity and density of melts of sodium disilicate, sodium metasilicate and diopside composition with pressure. *Carnegie Inst. Wash. Year Book, 78,* 547–551.

Seifert, F., D. Virgo and B. O. Mysen (1979) Melt structures and redox equilibria in the system Na_2O–FeO–Fe_2O_3–Al_2O_3–SiO_2. *Carnegie Inst. Wash. Year Book, 78,* 511–519.

Serna, C. J., B. D. Velde and J. L. White (1977) Infrared evidence of order–disorder in amesites. *Am. Mineral., 62,* 296–303.

———, J. L. White and B. D. Velde (1979) The effect of aluminum on the infrared spectra of trioctahedral minerals. *Mineral. Mag., 43,* 141–148.

Serratosa, J. M. and J. M. Vinas (1964) Infrared investigations of the OH-band in chlorites. *Nature, 202,* 999.

Sharma, S. K., D. Virgo and B. O. Mysen (1978) Structure of glasses and melts of $Na_2O \cdot xSiO_2$ (x = 1, 2, 3) composition from Raman spectroscopy. *Carnegie Inst. Wash. Year Book, 77,* 649–652.

Shaw, H. R. (1963) Obsidian–H_2O viscosities at 1000 and 2000 bars in the temperature range 700° to 900°C. *J. Geophys. Res., 68,* 6337–6343.

Stolen, R. H. and G. E. Walrafen (1976) Water and its relation to broken bond defects in fused silica. *J. Chem. Phys., 64,* 2623–2631.

Tarte, P. (1967) Infrared spectra of inorganic aluminates and characteristic vibrational frequencies of AlO_4 tetrahedra and AlO_6 octahedra. *Spectrochim. Acta, 23A,* 2127–2143.

Taylor, M. and G. E. Brown (1979) Structure of mineral glasses. I. The feldspar glasses $NaAlSi_3O_8$, $KAlSi_3O_8$, $CaAl_2Si_2O_8$. *Geochim. Cosmochim. Acta, 43,* 61–77.

Taylor, T. D. and G. E. Rindone (1970) Properties of soda aluminosilicate glasses. V. Low-temperature viscosities. *J. Am. Ceram. Soc., 53,* 692–695.

Uys, J. M. and T. B. King (1963) The effect of basicity on the solubility of water in silicate melts. *Trans. Metall. Soc. AIME, 227,* 492–500.

Van der Steen, G. H. A. M. and H. Van den Boom (1977) Raman study of hydrogen-containing vitreous silica. *J. Non-Cryst. Solids, 23,* 279–286.

Velde, B. D. and I. Kushiro (1976) Infrared spectra of high-pressure quenched silicate liquids. *Carnegie Inst. Wash. Year Book, 75,* 618–621.

Virgo, D., B. O. Mysen and F. Seifert (1979a) Structures of quenched melts in the system $NaAlSiO_4$–$CaMgSi_2O_6$–Mg_2SiO_4–SiO_2 at 1 atm. *Carnegie Inst. Wash. Year Book, 78,* 502–506.

———, F. Seifert and B. O. Mysen (1979b) Three-dimensional network structures of glasses in the systems $CaAl_2O_4$–SiO_2, $NaAlO_2$–SiO_2, $NaFeO_2$–SiO_2, and $NaGaO_2$–SiO_2 at 1 atm. *Carnegie Inst. Wash. Year Book, 78,* 506–511.

Wasserburg, G. J. (1957) The effects of H_2O in silicate systems. *J. Geol., 65,* 15–23.

Watson, E. B. (1976) Two-liquid partition coefficients: experimental data and geochemical implications. *Contrib. Mineral. Petrol., 56,* 119–134.

——— (1977) Partitioning of manganese between forsterite and silicate liquid. *Geochim. Cosmochim. Acta, 41,* 1363–1374.

Yoder, H. S., Jr. (1969) Calc-alkalic andesites: experimental data bearing on the origin of their assumed characteristics. In A. R. McBirney, Ed., *Proceedings of the Andesite Conference, Oreg. Dep. Geol. Miner. Ind. Bull., 65,* 77–89.

——— (1973) Contemporaneous basaltic and rhyolitic magmas. *Am. Mineral., 58,* 153–171.

Manuscript received, October 9, 1979;
accepted for publication, May 28, 1980.